

16 **Abstract**

17 Fire emissions influence radiation, climate, and ecosystems through aerosol radiative effects.
18 Meanwhile, these instantaneous environmental perturbations can feed back to affect fire emissions.
19 However, the magnitude of such feedback remains unclear on the global scale. Here, we quantify
20 the impacts of fire aerosols on climate through direct, indirect, and albedo effects based on the two-
21 way simulations using a well-established chemistry-climate-vegetation model. Globally, fire
22 emissions cause a reduction of $0.565 \pm 0.166 \text{ W m}^{-2}$ in net radiation at the top of the atmosphere with
23 dominant contributions by aerosol indirect effect (AIE). Consequently, terrestrial surface air
24 temperature decreases by $0.061 \pm 0.165 \text{ }^\circ\text{C}$ with coolings of $>0.25^\circ\text{C}$ over eastern Amazon, western
25 U.S., and boreal Asia. Both aerosol direct effect (ADE) and AIE contribute to such cooling while
26 the aerosol albedo effect (AAE) exerts an offset warming, especially at high latitudes. Land
27 precipitation decreases by $0.180 \pm 0.966 \text{ mm month}^{-1}$ ($1.78 \pm 9.56\%$) mainly due to the inhibition
28 in central Africa by AIE. Such rainfall deficit further reduces regional leaf area index (LAI) and
29 lightning ignitions, leading to changes in fire emissions. Globally, fire emissions reduce by 2%-3%
30 because of the fire-induced fast responses in humidity, lightning, and LAI. The fire aerosol radiative
31 effects may cause larger perturbations to climate systems with likely more fires under global
32 warming.

33

34 **Short summary**

35 We quantify the impacts of fire aerosols on climate through direct, indirect, and albedo effects.
36 We find global fire aerosols cause cooling of surface air temperature and inhibition of precipitation.
37 These climatic perturbations further reduce regional leaf area index and lightning ignitions, both of
38 which are not beneficial for fire emissions. By considering the feedback of fire aerosols on humidity,
39 lightning, and leaf area index, we predict a slight reduction in fire emissions.

40

41 **Keywords:** Fire emissions; radiative effect; climate feedback; ModelE2-YIBs model

42

43 **1 Introduction**

44 Fire occurs all year round in both hemispheres, burning about 1% of the Earth's surface and
45 emitting roughly 2–3 Pg ($=10^{15}$ g) carbon into atmosphere every year (van der Werf *et al.*, 2017).
46 Fire activities are strongly influenced by fuel availability, ignition/suppression, and climate
47 conditions (Flannigan *et al.*, 2009). The fuel type, continuity, and amount affect fire occurrence and
48 spread probability (Flannigan *et al.*, 2013). Lightning discharge is the most important natural source
49 of fire ignition (Macias Fauria and Johnson, 2006). Human activities affect fire patterns by adding
50 ignition sources or by suppressing processes (Andela *et al.*, 2017). Compared to the above factors,
51 climate shows a more dominant role in modulating fire activities through the changes of fuel
52 moisture and spread conditions (Flannigan and Harrington, 1988).

53 Fire exerts prominent impacts on Earth systems and human society through various processes.
54 Biomass burning emits a large amount of trace gases and aerosol particles into the troposphere,
55 affecting air quality at the local and downwind regions (Yue and Unger, 2018). *In situ* observations
56 showed that about one-third of the background particles in the free troposphere of North America
57 were originated from biomass burning (Hudson *et al.*, 2004). Extremely intense fires can even inject
58 aerosols into stratosphere, where the particles were transported globally (Yu *et al.*, 2019). Fire-
59 induced air pollution can reduce global terrestrial productivity of unburned forests (Yue and Unger,
60 2018), leading to weakened carbon uptake by ecosystems. The global transport of fire air pollution
61 also causes large threats to public health by increasing the risks of diseases and mortality (Liu *et al.*,
62 2015). It is estimated that fire-induced particulate matter causes more than 33,000 deaths globally
63 each year (Chen *et al.*, 2021).

64 Aerosols from fires can cause substantial impact on climate via radiative effect owing to their
65 different optical and chemical properties (Xu *et al.*, 2021). Aerosol radiative effect is the
66 instantaneous radiative impact on energy balance of climate system, representing the fast adjustment
67 or response before changing global mean surface air temperature (TAS). First, aerosols scatter
68 and/or absorb solar radiation through aerosol direct effect (ADE), leading to altered energy budget
69 and climate variables (Carslaw *et al.*, 2010). There is no agreement on the sign of ADE of biomass
70 burning aerosols at the global scale. Some studies (Heald *et al.*, 2014; Veira *et al.*, 2015; Zou *et al.*,
71 2020) predicted positive forcing while others (Ward *et al.*, 2012; Jiang *et al.*, 2016; Grandey *et al.*,
72 2016) yielded negative forcing (-0.2 to 0.2 W m^{-2}), mainly because of the large uncertainties in the

73 absorption of fire-emitted black carbon (BC) (Carslaw *et al.*, 2010; IPCC, 2014). Second, aerosols
74 can serve as cloud condensation nuclei (CCN) or ice nuclei to affect the microphysical properties
75 of cloud. Such aerosol indirect effect (AIE) further influences climate system through the changes
76 of cloud albedo and lifetime (Twomey, 1974; Albrecht, 1989). Globally, fire aerosols account for
77 ~30% of the total CCN (Andreae *et al.*, 2004) and the overall negative AIE of fire aerosol is stronger
78 than the ADE in magnitude (Liu *et al.*, 2014; Ward *et al.*, 2012; Jiang *et al.*, 2016). Third, deposition
79 of fire-emitted BC aerosols reduces surface albedo and promotes ice/snow melting, which is called
80 aerosol albedo effect (AAE) (Hansen and Nazarenko, 2004; Warren and Wiscombe, 1980).
81 Compared with other two effects, the AAE shows more regional characteristics (Kang *et al.*, 2020).
82 These fire-induced disturbance in radiative fluxes further alter meteorological and hydrologic
83 variables, which in turn affect fire activities through the changes in fuel moisture and weather
84 conditions.

85 Impact of fire-induced instantaneous climatic perturbations to fire activities on the global scale
86 have not been fully assessed. While observations revealed fire-induced perturbations to regional
87 climate (Bali *et al.*, 2017; Zhuravleva *et al.*, 2017), its feedback to fire activities are difficult to be
88 isolated from the influences of background climate. Models provide unique tools to explore fire-
89 climate interactions resulting from aerosol radiative effect especially at the regional to global scales.
90 However, they are not routinely included in most of Earth system models. The IPCC sixth
91 assessment report (AR6) did not provide a quantitative assessment of such feedback as well (IPCC,
92 2021). In this study, we explore the impacts of fire aerosol radiative effect on climate and the
93 consequent feedbacks to fire emissions by using a well-established fire parameterization coupled to
94 a chemistry-climate-vegetation model ModelE2-YIBs (Yue and Unger, 2015). The main objectives
95 are (1) to isolate the radiative effects of fire aerosols through ADE, AIE, and AAE processes and (2)
96 to quantify the feedback of fire-induced instantaneous climate effects to fire emissions.

97

98 **2 Data and methods**

99 **2.1 Data**

100 We use the emissions from Global Fire Emission Database version 4.1s (GFED4.1s) to validate
101 the simulated fire emissions. The GFED4.1s provides monthly fire emission fluxes of various air
102 pollutants based on satellite retrieval of area burned from the Moderate Resolution Imaging

103 Spectroradiometer (MODIS) (van der Werf *et al.*, 2017). Area burned in GFED4.1s is mainly
104 derived from the MODIS burned area product (Giglio *et al.*, 2013), taking into account "small" fires
105 outside the burned area maps based on active fire detections (Randerson *et al.*, 2012). The gridded
106 fire emission dataset has a spatial resolution of $0.25^\circ \times 0.25^\circ$ and is available for every month from
107 July 1997. To compute anthropogenic ignition and suppression effects (see section 2.3), we use a
108 downscaled population density dataset from Gao (2017, 2020). Monthly sea surface temperature
109 (SST) and sea ice concentration (SIC) obtained from Hadley Centre Sea Ice and Sea Surface
110 Temperature (HadISST) dataset (Rayner *et al.*, 2003) are used as the boundary conditions for the
111 climate model.

112

113 **2.2 ModelE2-YIBs model**

114 The chemistry-climate-vegetation model ModelE2-YIBs is used to simulate the two-way
115 coupling between fire aerosols and climate systems. The ModelE2-YIBs is composed of the NASA
116 Goddard Institute for Space Studies (GISS) ModelE2 model (Schmidt *et al.*, 2014) and the Yale
117 Interactive terrestrial Biosphere Model (YIBs) (Yue and Unger, 2015). The GISS ModelE2 is a
118 global climate-chemistry model with a horizontal resolution of $2^\circ \times 2.5^\circ$ latitude by longitude and
119 40 vertical layers extending to the stratosphere (0.1hPa). The dynamics and physics codes are
120 executed every 30 minutes and the radiation code is calculated every 2.5 hours.

121 The gas-phase chemistry scheme considers 156 chemical reactions among 51 species,
122 including NO_x - HO_x - O_x - CO - CH_4 chemistry and different species of volatile organic compounds.
123 Aerosol species in ModelE2 include sulfate, nitrate, sea salt, dust, BC, and organic carbon (OC),
124 which are interactively calculated and tracked for both mass and number concentrations. The aerosol
125 microphysical scheme is based on the quadrature method of moments, which incorporates
126 nucleation, gas-particle mass transfer, new particle formation, particle emissions, aerosol phase
127 chemistry, condensational growth, and coagulation (Bauer *et al.*, 2008). The residence time of
128 aerosol species varies greatly in space and time due to different removal rates. Turbulent dry
129 deposition is determined by resistance-in-series scheme, which is closely coupled to the boundary
130 layer scheme and implemented between the surface layer (10 m) and the ground (Koch *et al.*, 2006).
131 The wet deposition consists of several processes including scavenging within and below cloud,
132 evaporation of falling rainout, transportation along convective plumes, and detrainment and

133 evaporation from convective plumes (Koch *et al.*, 2006; Shindell *et al.*, 2006).

134 In ModelE2, gases can be converted to aerosols through chemical reactions, while aerosols
135 affect photolysis and provide reaction surface for gases. For example, the formation of sulfate
136 aerosols is driven by modeled oxidants (Bell *et al.*, 2005), and the chemical production of nitrate
137 aerosols is dependent on nitric acid and gaseous ammonia (Bauer *et al.*, 2007). Moreover, the
138 disturbances of aerosols on climate systems via direct, indirect, and albedo effects are considered in
139 ModelE2. Size-dependent optical parameters of aerosols are calculated by the Mie scattering theory.
140 The first AIE is estimated by the prognostic treatment of cloud droplet number concentration, which
141 is a function of contact nucleation, auto-conversion, and immersion freezing (Menon *et al.*, 2008;
142 Menon *et al.*, 2010). The AAE of BC is considered by estimating the decline of surface albedo as a
143 function of aerosol concentrations at the top layer of snow or ice (Koch and Hansen, 2005). BC
144 content in snow is determined by measurement-based average scavenging ratios (Hansen and
145 Nazarenko, 2004). More detailed descriptions of ModelE2 can be found in Schmidt *et al.* (2014). It
146 has been extensively evaluated for meteorological and chemical variables against observations,
147 reanalysis products and other models, and widely used for studies of climate systems, atmospheric
148 components, and their interactions (Schmidt *et al.*, 2014).

149 YIBs is a process-based vegetation model that dynamically simulates tree growth and
150 terrestrial carbon fluxes with prescribed fractions of nine plant functional types (PFTs), including
151 deciduous broadleaf forest, evergreen needleleaf forest, evergreen broadleaf forest, tundra,
152 shrubland, C₃/C₄ grassland, and C₃/C₄ cropland. Essential biological processes such as
153 photosynthesis, phenology, autotrophic and heterotrophic respiration are considered and
154 parameterized using the state-of-the-art schemes (Yue and Unger, 2015). Dynamic daily leaf area
155 index (LAI) is estimated based on carbon allocation and prognostic phenology which is dependent
156 on temperature and drought conditions. Simulated tree height, phenology, gross primary
157 productivity and LAI agree well with site-level observations and/or satellite retrievals (Yue and
158 Unger, 2015). The YIBs model joined the dynamic global vegetation model inter-comparison
159 project TRENDY and showed reasonable performance of carbon fluxes against available
160 observations (Friedlingstein *et al.*, 2020). In the coupled model, ModelE2 provides meteorological
161 drivers to YIBs, which feeds back to alter land surface water and energy fluxes through changes in
162 stomatal conductance, surface albedo, and LAI. By incorporating YIBs into ModelE2, the new

163 coupled model ModelE2-YIBs can simulate interactions between terrestrial ecosystems and climate
 164 systems through the exchange of water and energy fluxes, and chemical components (Yue and Unger,
 165 2015; Yue *et al.*, 2017).

166

167 2.3 Fire parameterization

168 We implemented the active global fire parameterization from Pechony and Shindell (2009) into
 169 ModelE2-YIBs model. The parameterization considers key fire-related processes including fuel
 170 flammability, lightning and human ignitions, and human suppressions. Flammability is a unitless
 171 metric indicating conditions favorable for fire occurrence, and is calculated using vapor pressure
 172 deficit (VPD, hPa), precipitation (R, mm day⁻¹), and LAI (m² m⁻²) as follows:

$$173 \text{Flam} = \text{VPD} \times \text{LAI} \times e^{-c_R \times R} \quad (1)$$

174 Here, LAI represents vegetation density and is dynamically calculated by YIBs model. c_R is a
 175 constant set to 2. VPD is a vital indicator of flammability conditions:

$$176 \text{VPD} = e_s \times \left(1 - \frac{\text{RH}}{100}\right) \quad (2)$$

177 where e_s is the saturation vapor pressure and RH is surface relative humidity. e_s can be
 178 calculated by Goff-Gratch equation:

$$179 e_s = e_{st} \times 10^Z \quad (3)$$

180 where e_{st} is 1013.246 hPa and

$$181 Z = a \times \left(\frac{T_s}{T} - 1\right) + b \times \log \frac{T_s}{T} + c \times \left(10^{d\left(1 - \frac{T_s}{T}\right)} - 1\right) + f \times \left(10^{h\left(\frac{T_s}{T} - 1\right)} - 1\right) \quad (4)$$

182 Here, a, b, c, d, f and h are constants set to -7.90298, 5.02808, -1.3816×10⁻⁷, 11.344, 8.1328×10⁻³
 183 and -3.49149, respectively. T_s is boiling point of water and equal to 373.16 K. VPD and LAI in Eq.
 184 (1) are calculated in half-hourly and daily time step, respectively, while 30-day running average
 185 precipitation is employed to avoid unrealistically huge flammability fluctuations.

186 Natural and anthropogenic ignition determines whether the fire can actually occur. If ignition
 187 is zero, the resulting fire emissions will be zero, regardless of flammability. Natural ignition source
 188 I_N depends on cloud-to-ground lightning (CoGL) rate, which is simulated by ModelE2 following
 189 the parameterization of Price and Rind (1994):

$$190 I_N = \text{CoGL} = \begin{cases} 3.44 \times 10^{-5} \times H^{4.9} & \text{over land} \\ 6.4 \times 10^{-4} \times H^{1.73} & \text{over ocean} \end{cases} \quad (5)$$

191 where H is the cloud depth (unit: km).

192 Humans influence fire activity by adding ignition sources and suppressing fire events, the rates
 193 of which increase with population and to some extent counteract each other. The number of
 194 anthropogenic ignition source I_A (number $\text{km}^{-2} \text{month}^{-1}$) is calculated as follows (Venevsky *et al.*,
 195 2002):

$$196 \quad I_A = k(\text{PD}) \times \text{PD} \times \alpha \quad (6)$$

197 where PD is population density (number km^{-2}). $k(\text{PD}) = 6.8 \times \text{PD}^{-0.6}$ stands for ignition
 198 potentials of human activity, assuming that people in scarcely populated areas interact more with
 199 the natural ecosystems and therefore produce more ignition potential. α is the number of potential
 200 ignitions per person per month and set to 0.03.

201 In principle, the successful suppression of fires is dependent on early detection. It is reasonably
 202 assumed that fires are detected earlier and suppressed more effectively in highly populated areas.
 203 Therefore, the fraction of non-suppressed fires F_{NS} can be expressed as:

$$204 \quad F_{\text{NS}} = c_1 + c_2 \times \exp(-\omega \times \text{PD}) \quad (7)$$

205 where c_1 , c_2 and ω are constants and set to 0.05, 0.95 and 0.05, respectively. The selection of
 206 constant values in Eq. (7) is done in a heuristic way, due to lack of quantified data globally. It
 207 assumes that up to 95% of fires is suppressed in the densely populated regions but only 5% in
 208 unpopulated areas.

209 With the calculation of flammability (Flam), ignition (I_N and I_A), and non-suppression (F_{NS}),
 210 the fire count density N_{fire} (unit: number km^{-2}) at a specific time step can be derived as:

$$211 \quad N_{\text{fire}} = \text{Flam} \times (I_N + I_A) \times F_{\text{NS}} \quad (8)$$

212 Finally, fire emissions of trace gases and particulate matters (FireEmis) are calculated as:

$$213 \quad \text{FireEmis} = N_{\text{fire}} \times \text{EF} \quad (9)$$

214 Here, EF is the PFT-specific emission factor of an air pollutant such as BC, OC, NO_x , NH_3 , SO_2 ,
 215 CO, Alkenes and Paraffin. For each species, simulated gridded emissions are grouped by dominant
 216 PFT and compared to annual total emissions from GFED4.1s over the same grids. The EF is then
 217 calibrated to minimize the root-mean-square error between the simulated and GFED data for all
 218 land grids. Such calibration adjusts only the global total amount of fire emissions without changing
 219 the spatiotemporal pattern predicted by the parameterization.

220 Compared to fire indexes, such as Canadian Fire Weather Index system (Wagner, 1987), this
 221 fire parameterization shows advantages in integrating the effects of meteorology, vegetation, natural

222 ignition, and human activities (both ignition and suppression) on fires. Furthermore, it is physically
223 straightforward and has been validated based on global observations (Pechony and Shindell, 2009).
224 In ModelE2-YIBs, fire emissions are affected by environmental factors following above
225 parameterizations. In turn, the radiative effects of fire-emitted aerosols feed back to affect those
226 climatic and ecological factors. We consider only the fire emissions at surface due to the large
227 uncertainties in depicting fire plume height (Sofiev *et al.*, 2012; Ke *et al.*, 2021). The fire emissions
228 include both primary aerosols and trace gases, the latter of which react with other species to form
229 the secondary aerosols. These particles could be transported across the globe by the three-
230 dimensional atmospheric circulation and eventually removed through either dry or wet deposition.

231

232 **2.4 Simulations**

233 We perform four groups of sensitivity experiments (Table 1) with the ModelE2-YIBs model to
234 quantify the fire-climate interactions through different radiative processes. The first group with
235 suffix ‘AD’ considers only the ADE. The second (third) group with suffix ‘AD_AI’ (‘AD_AA’)
236 considers both ADE and AIE (ADE and AAE). The fourth group with suffix ‘AD_AI_AA’ includes
237 all three aerosol radiative effects (ADE, AIE, and AAE). Within each group, two runs are performed
238 with (YF) or without (NF) fire emissions. For YF simulations, fire-induced aerosols including
239 primarily emitted and secondarily formed are dynamically calculated based on fire parameterization
240 (see section 2.3) and atmospheric transport. These fire emissions cause radiative perturbations and
241 the consequent changes in climatic variables, which feedback to influence fire emissions. For NF
242 simulations, fire emissions are calculated offline at each step without perturbing the climate system,
243 which can be considered that there is no fire emission. By comparing the climatic variables from
244 the YF and NF runs in the first group, we isolate the impacts of fire aerosols on climate through
245 ADE. By comparing the climatic effects from the first and second (third) groups, we isolate the AIE
246 (AAE) of fire aerosols. By comparing the climatic variables from YF and NF runs in the fourth
247 group, the overall effect (ADE+AIE+AAE) is obtained. Besides, the differences of fire emissions
248 between simulations of “YF_AD_AI_AA” and “NF_AD_AI_AA” represent the feedback of fire
249 aerosol-induced environmental perturbations.

250 For each simulation, climatological mean CO₂ concentrations, SST/SIC, and population
251 density during 1995-2005 are used as boundary conditions to drive the model. Such configuration

252 ignores the year-to-year variability in climate systems, which may cause significant changes in
253 annual fire emissions (Burton *et al.*, 2020). Each simulation is integrated for 25 years with the first
254 5 years spinning up and the last 20-year averaged. Two-tail student t-test is performed to assess 90%
255 confidence levels of the predicted radiative and climatic responses ($p < 0.1$). In this study, downward
256 (upward) radiative/heat fluxes are defined as positive (negative). Given that the model is driven by
257 prescribed SST and SIC, only the rapid adjustments of atmospheric variables are taken into account
258 and we mainly focus on climate changes over land grid. The radiative effect simulated with such
259 model configuration is termed the effective radiative forcing (ERF).

260

261 **3 Results**

262 **3.1 Model evaluation**

263 Simulated fire emissions of BC and OC show hotspots in the tropics, such as Amazon, Sahel,
264 central Africa, and Southeast Asia (Fig. S1). The large tropical fire emissions are related to abundant
265 vegetation and/or distinct dry seasons. Compared to GFED4.1s data, ModelE2-YIBs slightly
266 underestimates boreal fire emissions especially over northern Asia and North America. On the
267 global scale, fire releases 1.85 ± 0.01 Tg ($1 \text{ Tg} = 10^{12} \text{ g}$) C year⁻¹ of BC and 16.8 ± 0.92 Tg C year⁻¹
268 of OC in ModelE2-YIBs, close to the 1.86 Tg C year⁻¹ of BC and 16.4 Tg C year⁻¹ of OC estimated
269 by GFED4.1s. In general, ModelE2-YIBs reasonably captures the spatial distribution of fire
270 emissions, with high spatial correlations of 0.67 ($p < 0.01$) for BC and 0.58 ($p < 0.01$) for OC, and
271 low normalized mean biases of 0.6% for BC and 2.4% for OC against satellite-based observations.

272

273 **3.2 Fire-induced radiative perturbations**

274 Fig. S2 shows the fire-induced changes in Aerosol Optical Depth (AOD) at 550nm. Fire
275 emissions largely enhance surface aerosols especially over tropical regions. Hotspots are located in
276 southern Africa and South America with regional enhancement larger than 0.05 . In addition, large
277 enhancement is also found at boreal high latitudes (> 0.01). At the global scale, fires enhance AOD
278 by 0.006 ± 0.001 with 0.010 ± 0.001 over land.

279 Fire aerosols cause large perturbations in net radiation at top of atmosphere (TOA). Globally,
280 the net radiation at TOA decreases $0.565 \pm 0.166 \text{ W m}^{-2}$ by fire aerosols (Fig. 1a). Regionally,
281 negative changes are predicted over central Africa, western South America, western North America

282 and the boreal high latitudes. Diagnosis shows that fire-induced AIE dominates the reduction of
283 TOA flux with a global value of $-0.440 \pm 0.264 \text{ W m}^{-2}$ (Fig. 1c), accounting for 78% of the total
284 TOA radiative effect by fire aerosols. The spatial correlation coefficient is 0.62 over land grids
285 between the perturbations by all aerosol effects and that by AIE alone. Compared to AIE, the
286 changes in TOA radiative fluxes are much smaller for fire ADE ($-0.058 \pm 0.213 \text{ W m}^{-2}$, Fig. 1b) and
287 AAE ($-0.016 \pm 0.283 \text{ W m}^{-2}$, Fig. 1d) with limited perturbations on land.

288 Fire aerosols decrease net shortwave radiation reaching the surface up to 9 W m^{-2} in central
289 Africa and 7 W m^{-2} in Amazon (Fig. 2a), where biomass burning emissions are most intense (Fig.
290 S1). Such pattern is in general consistent with the changes of TOA fluxes (Fig. 1a), leading to an
291 average reduction of $-1.227 \pm 0.216 \text{ W m}^{-2}$ in the shortwave radiation over global land. The fire-
292 induced ADE alone reduces land surface shortwave radiation by $0.654 \pm 0.353 \text{ W m}^{-2}$ with the
293 maximum center in Amazon (Fig. S3a). As a comparison, the fire-induced AIE causes a smaller
294 reduction of $-0.553 \pm 0.518 \text{ W m}^{-2}$ with the hotspot in central Africa (Fig. S3c). The net effect of
295 AAE ($0.263 \pm 0.551 \text{ W m}^{-2}$) by fire aerosols is positive mainly because fire AAE reduces surface
296 albedo and increase shortwave radiation over Tibetan Plateau and boreal high latitudes (Fig. S3e).
297 However, the magnitude of AAE is much smaller compared to that of ADE and AIE.

298 Changes in surface longwave radiation (Fig. 2b) are much smaller than those in shortwave
299 radiation (Fig. 2a). Regionally, positive changes are predicted in the western U.S., eastern Amazon,
300 and South Africa, where fire-induced surface cooling (Fig. 3a) decreases the upward longwave
301 radiation. On the global scale, fire aerosols cause a decrease of $0.281 \pm 0.371 \text{ W m}^{-2}$ in surface
302 upward longwave radiation. As a result, fire aerosols induce a net atmospheric absorption of 0.191
303 $\pm 0.227 \text{ W m}^{-2}$ over land grids (Fig. 2c). The reductions in surface shortwave radiation are largely
304 balanced by changes in heat fluxes at the surface, which shows an average decrease of 0.826 ± 0.311
305 W m^{-2} in the upward fluxes over land grids (Fig. 2d). Fire ADE and AIE lead to reductions of 0.503
306 $\pm 0.289 \text{ W m}^{-2}$ and $0.432 \pm 0.411 \text{ W m}^{-2}$ in surface upward heat fluxes, respectively (Fig. S3b and
307 S3d). Changes in sensible heat account for 82.2 % of the changes in total heat reduction, much
308 higher than the contributions of 17.8% by latent heat fluxes (Fig. S4). Regionally, the upward
309 sensible heat decreases in the western U.S. and Amazon mainly due to fire ADE, while the upward
310 latent heat decreases in central Africa mainly by fire AIE (Fig. S5).

311

312 **3.3 Fire-induced fast climatic responses**

313 In response to the perturbations in radiative fluxes, land TAS decreases 0.061 ± 0.165 °C
314 globally by fire aerosols (Fig. 3a). Such cooling is mainly located in western U.S., Amazon, and
315 boreal Asia, following the large reductions in shortwave radiation (Fig. 2a). Meanwhile, moderate
316 warming is predicted at the high latitudes of both hemispheres especially over the areas covered
317 with land ice such as Greenland and Antarctica. Sensitivity experiments show that both ADE (Fig.
318 4a) and AIE (Fig. 4c) of fire aerosols result in net cooling globally, with regional reductions of TAS
319 over boreal Asia and North America. In contrast, the fire AAE causes increases of TAS over boreal
320 Asia and North America (Fig. 4e), where the deposition of BC aerosols reduces surface albedo.
321 Consequently, the fire AAE results in a global warming of 0.054 ± 0.163 °C, which in part offsets
322 the cooling effects by the ADE and AIE of fire aerosols.

323 Meanwhile, global land precipitation decreases by 0.180 ± 0.966 mm/month ($1.78 \pm 9.56\%$)
324 with great spatial heterogeneity (Fig. 3b). Decreased precipitation is predicted over central Africa,
325 boreal North America, and eastern Siberia. In contrast, increased rainfall is predicted in western
326 U.S., eastern Amazon, and northern Asia. The reduction of precipitation is mainly contributed by
327 fire AIE, which reduces cloud droplet size and inhibits local rainfall in central Africa (Fig. 4d).
328 Consequently, latent heat fluxes are reduced to compensate the rainfall deficit in central Africa (Fig.
329 S4b).

330

331 **3.4 Climate feedback to fire aerosol radiative effect**

332 The fire-aerosol-induced fast response in precipitation, VPD, lightning, and LAI can feed back
333 to affect fire emissions. However, these changes may have contrasting impacts on fire activities. For
334 example, the aerosol-induced reduction of precipitation in central Africa (Fig. 3b) increases local
335 VPD (Fig. 5a) and consequently causes more fire emissions. Meanwhile, such enhanced drought
336 condition inhibits plant growth and decreases local LAI (Fig. 5c), which has negative impacts on
337 fire emissions by reducing fuel density. Furthermore, the fire AIE inhibits the development of
338 convective cloud, which limits cloud height and the number of cloud-to-ground lightning in central
339 Africa (Fig. 5b), leading to reduced ignition sources and fire emissions.

340 To illustrate the joint the impacts of fire-aerosol-induced instantaneous climatic change, we
341 count the number out of the four factors contributing positive effects to fire emissions over land

342 grids (Fig. 5d). The larger (smaller) number indicates higher possibility of increasing (decreasing)
343 fire emissions. Most of areas show neutral number of 2, indicating offsetting effects of the changes
344 in fire-prone factors. Only 13.5 % of land grids show numbers higher than 2 with sparse distribution.
345 In contrast, 32.1 % of land grids show numbers smaller than 2, especially for the grids over Siberia
346 and western U.S. where the increased rainfall (Fig. 3b) and decreased VPD (Fig. 5a) inhibit fire
347 emissions. Furthermore, the regional reductions in lightning ignition or LAI promote the inhibition
348 effects. As a result, fire emissions in YF_AD_AI_AA slightly decrease by $31.0 \pm 35.9 \text{ Gg year}^{-1}$
349 (1.7%) for BC and $493.6 \pm 566.8 \text{ Gg year}^{-1}$ (2.9%) for OC compared to NF_AD_AI_AA in which
350 fire emissions do not perturb climate (Fig. 6).

351

352 **4 Conclusions and discussion**

353 We used the chemistry-climate-vegetation coupled model ModelE2-YIBs to quantify fire-
354 climate interactions through ADE, AIE, and AAE. Globally, fire aerosols decrease TOA net radiation
355 by $0.565 \pm 0.166 \text{ W m}^{-2}$, dominated by the AIE over central Africa. Surface net solar radiation also
356 exhibits widespread reductions especially over fire-prone areas with compensations from the
357 decreased sensible and latent heat fluxes. Following the changes in radiation, land TAS decreases
358 by $0.061 \pm 0.165 \text{ }^{\circ}\text{C}$ and precipitation decreases by $0.180 \pm 0.966 \text{ mm/month}$, albeit with regional
359 inconsistencies. The surface cooling is dominated by fire ADE and AIE, while the drought tendency
360 is mainly contributed by fire AIE with hotspots in central Africa. AAE also plays an important role
361 by introducing warming tendency at the mid-to-high latitudes. These fire-induced fast climatic
362 responses further affect VPD, LAI, and lightning ignitions, leading to reductions in global fire
363 emissions of BC by 2% and OC by 3%.

364 Our predicted reduction of $0.565 \pm 0.166 \text{ W m}^{-2}$ in TOA radiation by fire aerosols is close to
365 the estimate of -0.51 W m^{-2} reported by Jiang *et al.* (2016) and -0.59 W m^{-2} of Zou *et al.* (2020)
366 using different models with prescribed SST/SIC and fire-induced ADE, AIE and AAE (Table 2).
367 Within such change, fire ADE alone makes a moderate contribution of $-0.016 \pm 0.283 \text{ W m}^{-2}$, falling
368 within the range of -0.2 to 0.2 W m^{-2} from other studies. The large uncertainty of fire ADE is likely
369 related to the discrepancies in the BC absorption among climate models, which cause varied net
370 effects when offsetting the radiative perturbations of scattering aerosols. As a comparison, fire AIE
371 in our model induces a significant radiative effect of $-0.440 \pm 0.264 \text{ W m}^{-2}$. However, such

372 magnitude is much smaller than previous estimates of -0.7 to -1.1 W m^{-2} using different models
373 (Table 2). We further estimated a limited fire AAE of $-0.016 \pm 0.283 \text{ W m}^{-2}$, consistent with previous
374 findings showing insignificant role of AAE by fire aerosols (Ward *et al.*, 2012; Jiang *et al.*, 2016).
375 Our estimates of reductions in TAS and precipitation also fall within the range of previous studies
376 (Table 2).

377 Our estimates are subject to some limitations and uncertainties. First, we considered only the
378 fast climatic responses of land surface with prescribed SST and SIC in the simulations. Although
379 most of fire-induced AOD changes are located on land (Fig. S2), the air-sea interaction may cause
380 complex climatic responses to aerosol radiative effects. In a recent study, Jiang *et al.* (2020)
381 emphasized the role of slow feedback contributed by fire aerosols on global precipitation reduction
382 by using a coupled model. Such air-sea interaction will modify the magnitude and/or spatial pattern
383 of fast climatic responses revealed in this study, and should be explored in the future studies with
384 coupled ocean models. Second, the nonlinear effects of different radiative processes may influence
385 the attribution results. In this study, we isolate the effects of AIE and AAE by subtracting variables
386 between different groups following the approaches by Bauer and Menon (2012). However, the
387 additive perturbations from individual processes are not equal to the total perturbations with all
388 processes in one simulation. For example, the sum of three processes causes changes of TOA
389 radiation by $-0.513 \pm 0.324 \text{ W m}^{-2}$ (Figs 1b-1d), surface temperature by $-0.037 \pm 0.160 \text{ }^{\circ}\text{C}$ (Figs 4a,
390 4c, 4e), and precipitation by $-1.090 \pm 1.122 \text{ mm month}^{-1}$ (Figs 4b, 4d, 4f). These perturbations are
391 weaker than the net effects of $0.565 \pm 0.166 \text{ W m}^{-2}$ (Fig. 1a) in radiation and $-0.061 \pm 0.165 \text{ }^{\circ}\text{C}$ in
392 temperature (Fig. 3a), but much stronger than that of $-0.18 \pm 0.96 \text{ mm month}^{-1}$ in precipitation (Fig.
393 3b) predicted by the simulation with all three processes. As a result, the nonlinear feedbacks among
394 different radiative processes may magnify or offset the final climatic responses to fire aerosols.
395 Third, considering the complex nature of fire activities, the fire parameterization in this study does
396 not incorporate all fire-related processes (e.g., the influence of wind). In addition, the simulations
397 omit several factors influencing fire emissions (e.g., moist content of fuels) and aerosol radiative
398 effects (e.g. fire plume height). For example, studies show significant impacts of plume rise on the
399 vertical distribution of fire aerosols and the consequent radiative effects (Walter *et al.*, 2016). The
400 impacts of human activity on fire emissions are calculated as a function of population density
401 without considerations of differences in economy, education, and policies. These auxiliary factors

402 may increase the spatial heterogeneity of fire aerosol radiative effects and deserve further
403 explorations in the future studies.

404 Despite these limitations, we made the first attempt to assess the two-way interaction between
405 fire emissions and climate via aerosol radiative effects. Our results show that fire-emitted aerosols
406 cause negative ERF of $0.565 \pm 0.166 \text{ W m}^{-2}$, which is about 20% of the anthropogenic ERF due to
407 the increased greenhouse gases and aerosols from 1950 to 2019 (IPCC, 2021). Such fire ERF largely
408 reduces regional TAS and precipitation, leading to further changes in fire emissions. Although the
409 reduction of 2% to 3% in fire emissions by the fire-climate interaction through aerosol radiative
410 effect seems limited, such change is a result of several complex feedbacks that may exert offsetting
411 effects. Furthermore, our simulations reveal a strong inhibition effect of fire aerosols on LAI in
412 central Africa due to the aerosol-induced drought intensification. Such negative effects on
413 ecosystems are inconsistent with previous estimates that showed certain fertilization effects by fire
414 aerosols (Yue and Unger, 2018), mainly because the rainfall deficit overweighs the diffuse
415 fertilization effects of aerosols. With likely more fires under global warming (Abatzoglou *et al.*,
416 2019), our results suggested complex and uncertain perturbations by fire emissions to climate and
417 ecosystem through fire-climate interactions.

418

419 **Acknowledgements**

420 The authors are grateful to Dr. Matthew Kasoar and another anonymous reviewer for their
421 constructive comments that have improved this study.

422

423 **Financial support**

424 This research was supported by the National Key Research and Development Program of China
425 (grant no. 2019YFA0606802).

426

427 **Competing Interests**

428 The authors declare that they have no conflict of interest.

429

430 **Data availability**

431 Hadley Centre Sea Ice and Sea Surface Temperature dataset were obtain from

432 <https://www.metoffice.gov.uk/hadobs/hadisst/>. Population data could be downloaded from
433 <https://cmr.earthdata.nasa.gov/search/concepts/C1739468823-SEDAC.html>. GFED data were
434 obtained from https://daac.ornl.gov/VEGETATION/guides/fire_emissions_v4_R1.html.
435

436 **Reference:**

- 437 Abatzoglou J T, Williams A P and Barbero R 2019 Global Emergence of Anthropogenic Climate Change
438 in Fire Weather Indices *Geophysical Research Letters* **46** 326-36
- 439 Albrecht B A 1989 Aerosols, Cloud Microphysics, and Fractional Cloudiness **245** 1227-30
- 440 Andela N, Morton D C, Giglio L, Chen Y, van der Werf G R, Kasibhatla P S, DeFries R S, Collatz G J,
441 Hantson S, Kloster S, Bachelet D, Forrest M, Lasslop G, Li F, Mangeon S, Melton J R, Yue C
442 and Randerson J T 2017 A human-driven decline in global burned area *Science* **356** 1356
- 443 Andreae M O, Rosenfeld D, Artaxo P, Costa A A, Frank G P, Longo K M and Silva-Dias M A F 2004
444 Smoking Rain Clouds over the Amazon **303** 1337-42
- 445 Bali K, Mishra A K and Singh S 2017 Impact of anomalous forest fire on aerosol radiative forcing and
446 snow cover over Himalayan region *Atmospheric Environment* **150** 264-75
- 447 Bauer S E and Menon S 2012 Aerosol direct, indirect, semidirect, and surface albedo effects from sector
448 contributions based on the IPCC AR5 emissions for preindustrial and present-day conditions
449 **117**
- 450 Bauer S E, Mishchenko M I, Laci A A, Zhang S, Perlwitz J and Metzger S M 2007 Do sulfate and nitrate
451 coatings on mineral dust have important effects on radiative properties and climate modeling?
452 **112**
- 453 Bauer S E, Wright D L, Koch D, Lewis E R, McGraw R, Chang L S, Schwartz S E and Ruedy R 2008
454 MATRIX (Multiconfiguration Aerosol TRacker of mIXing state): an aerosol microphysical
455 module for global atmospheric models *Atmos. Chem. Phys.* **8** 6003-35
- 456 Bell N, Koch D and Shindell D T 2005 Impacts of chemistry-aerosol coupling on tropospheric ozone and
457 sulfate simulations in a general circulation model **110**
- 458 Burton C, Betts R A, Jones C D, Feldpausch T R, Cardoso M and Anderson L O 2020 El Niño Driven
459 Changes in Global Fire 2015/16 **8**
- 460 Carslaw K S, Boucher O, Spracklen D V, Mann G W, Rae J G L, Woodward S and Kulmala M 2010 A
461 review of natural aerosol interactions and feedbacks within the Earth system *Atmos. Chem. Phys.*
462 **10** 1701-37
- 463 Chen G, Guo Y, Yue X, Tong S, Gasparrini A, Bell M L, Armstrong B, Schwartz J, Jaakkola J J K,
464 Zanutti A, Lavigne E, Nascimento Saldiva P H, Kan H, Royé D, Milojevic A, Overcenco A,
465 Urban A, Schneider A, Entezari A, Vicedo-Cabrera A M, Zeka A, Tobias A, Nunes B, Alahmad
466 B, Forsberg B, Pan S-C, Íñiguez C, Ameling C, De la Cruz Valencia C, Åström C, Houthuijs D,
467 Van Dung D, Samoli E, Mayvaneh F, Sera F, Carrasco-Escobar G, Lei Y, Orru H, Kim H,
468 Holobaca I-H, Kyselý J, Teixeira J P, Madureira J, Katsouyanni K, Hurtado-Díaz M,
469 Maasikmets M, Ragettli M S, Hashizume M, Stafoggia M, Pascal M, Scortichini M, de Sousa
470 Zanotti Stagliorio Coêlho M, Valdés Ortega N, Rytí N R I, Scovronick N, Matus P, Goodman P,
471 Garland R M, Abrutzky R, Garcia S O, Rao S, Fratianni S, Dang T N, Colistro V, Huber V, Lee
472 W, Seposo X, Honda Y, Guo Y L, Ye T, Yu W, Abramson M J, Samet J M and Li S 2021 Mortality
473 risk attributable to wildfire-related PM_{2.5} pollution: a global time series
474 study in 749 locations *The Lancet Planetary Health* **5** e579-e87
- 475 Flannigan M, Cantin A S, de Groot W J, Wotton M, Newbery A and Gowman L M 2013 Global wildland
476 fire season severity in the 21st century *Forest Ecology and Management* **294** 54-61
- 477 Flannigan M and Harrington J B 1988 A Study of the Relation of Meteorological Variables to Monthly
478 Provincial Area Burned by Wildfire in Canada (1953–80) *Journal of Applied Meteorology and
479 Climatology* **27** 441-52

480 Flannigan M, Krawchuk M A, de Groot W J, Wotton B M and Gowman L M 2009 Implications of
481 changing climate for global wildland fire %J *International Journal of Wildland Fire* **18** 483-507

482 Friedlingstein P, O'Sullivan M, Jones M W, Andrew R M, Hauck J, Olsen A, Peters G P, Peters W,
483 Pongratz J, Sitch S, Le Quéré C, Canadell J G, Ciais P, Jackson R B, Alin S, Aragão L E O C,
484 Arneeth A, Arora V, Bates N R, Becker M, Benoit-Cattin A, Bittig H C, Bopp L, Bultan S,
485 Chandra N, Chevallier F, Chini L P, Evans W, Florentie L, Forster P M, Gasser T, Gehlen M,
486 Gilfillan D, Gkritzalis T, Gregor L, Gruber N, Harris I, Hartung K, Haverd V, Houghton R A,
487 Ilyina T, Jain A K, Joetzjer E, Kadono K, Kato E, Kitidis V, Korsbakken J I, Landschützer P,
488 Lefèvre N, Lenton A, Lienert S, Liu Z, Lombardozzi D, Marland G, Metzl N, Munro D R, Nabel
489 J E M S, Nakaoka S I, Niwa Y, O'Brien K, Ono T, Palmer P I, Pierrot D, Poulter B, Resplandy
490 L, Robertson E, Rödenbeck C, Schwinger J, Séférian R, Skjelvan I, Smith A J P, Sutton A J,
491 Tanhua T, Tans P P, Tian H, Tilbrook B, van der Werf G, Vuichard N, Walker A P, Wanninkhof
492 R, Watson A J, Willis D, Wiltshire A J, Yuan W, Yue X and Zaehle S 2020 Global Carbon Budget
493 2020 *Earth Syst. Sci. Data* **12** 3269-340

494 Gao J 2017 Downscaling Global Spatial Population Projections from 1/8-degree to 1-km Grid Cells.

495 Gao J 2020 Global 1-km Downscaled Population Base Year and Projection Grids Based on the Shared
496 Socioeconomic Pathways, Revision 01. (Palisades, NY: NASA Socioeconomic Data and
497 Applications Center (SEDAC))

498 Giglio L, Randerson J T and van der Werf G R 2013 Analysis of daily, monthly, and annual burned area
499 using the fourth-generation global fire emissions database (GFED4) *Journal of Geophysical*
500 *Research: Biogeosciences* **118** 317-28

501 Grandey B S, Lee H H and Wang C 2016 Radiative effects of interannually varying vs. interannually
502 invariant aerosol emissions from fires *Atmos. Chem. Phys.* **16** 14495-513

503 Hansen J and Nazarenko L 2004 Soot climate forcing via snow and ice albedos **101** 423-8

504 Heald C L, Ridley D A, Kroll J H, Barrett S R H, Cady-Pereira K E, Alvarado M J and Holmes C D 2014
505 Contrasting the direct radiative effect and direct radiative forcing of aerosols *Atmos. Chem. Phys.*
506 **14** 5513-27

507 Hudson P K, Murphy D M, Cziczko D J, Thomson D S, de Gouw J A, Warneke C, Holloway J, Jost H-J
508 and Hübler G 2004 Biomass-burning particle measurements: Characteristic composition and
509 chemical processing **109**

510 IPCC 2014 *Contribution of Working Groups I, II and III to the Fifth Assessment Report of the*
511 *Intergovernmental Panel on Climate Change [Core Writing Team, R.K. Pachauri and L.A.*
512 *Meyer (eds.)]* (IPCC, Geneva, Switzerland)

513 IPCC 2021 *Climate Change 2021: The Physical Science Basis. Contribution of Working Group I to the*
514 *Sixth Assessment Report of the Intergovernmental Panel on Climate Change [Masson-Delmotte,*
515 *V., P. Zhai, A. Pirani, S. L. Connors, C. Péan, S. Berger, N. Caud, Y. Chen, L. Goldfarb, M. I.*
516 *Gomis, M. Huang, K. Leitzell, E. Lonnoy, J. B. R. Matthews, T. K. Maycock, T. Waterfield, O.*
517 *Yelekçi, R. Yu and B. Zhou (eds.)]* vol In Press.: Cambridge University Press.)

518 Jiang Y, Lu Z, Liu X, Qian Y, Zhang K, Wang Y and Yang X Q 2016 Impacts of global open-fire aerosols
519 on direct radiative, cloud and surface-albedo effects simulated with CAM5 *Atmos. Chem. Phys.*
520 **16** 14805-24

521 Jiang Y, Yang X-Q, Liu X, Qian Y, Zhang K, Wang M, Li F, Wang Y and Lu Z 2020 Impacts of Wildfire
522 Aerosols on Global Energy Budget and Climate: The Role of Climate Feedbacks *Journal of*
523 *Climate* **33** 3351-66

- 524 Kang S, Zhang Y, Qian Y and Wang H 2020 A review of black carbon in snow and ice and its impact on
525 the cryosphere *Earth-Science Reviews* **210** 103346
- 526 Ke Z, Wang Y, Zou Y, Song Y and Liu Y 2021 Global Wildfire Plume-Rise Data Set and
527 Parameterizations for Climate Model Applications **126** e2020JD033085
- 528 Koch D and Hansen J 2005 Distant origins of Arctic black carbon: A Goddard Institute for Space Studies
529 ModelE experiment *Journal of Geophysical Research: Atmospheres* **110**
- 530 Koch D, Schmidt G A and Field C V 2006 Sulfur, sea salt, and radionuclide aerosols in GISS ModelE
531 **111**
- 532 Liu J C, Pereira G, Uhl S A, Bravo M A and Bell M L 2015 A systematic review of the physical health
533 impacts from non-occupational exposure to wildfire smoke *Environmental Research* **136** 120-
534 32
- 535 Liu Y, Goodrick S and Heilman W 2014 Wildland fire emissions, carbon, and climate: Wildfire–climate
536 interactions *Forest Ecology and Management* **317** 80-96
- 537 Macias Fauria M and Johnson E A 2006 Large-scale climatic patterns control large lightning fire
538 occurrence in Canada and Alaska forest regions *Journal of Geophysical Research:*
539 *Biogeosciences* **111**
- 540 Menon S, Del Genio A D, Kaufman Y, Bennartz R, Koch D, Loeb N and Orlikowski D 2008 Analyzing
541 signatures of aerosol-cloud interactions from satellite retrievals and the GISS GCM to constrain
542 the aerosol indirect effect **113**
- 543 Menon S, Koch D, Beig G, Sahu S, Fasullo J and Orlikowski D 2010 Black carbon aerosols and the third
544 polar ice cap *Atmos. Chem. Phys.* **10** 4559-71
- 545 Pechony O and Shindell D T 2009 Fire parameterization on a global scale *Journal of Geophysical*
546 *Research* **114**
- 547 Price C and Rind D 1994 Modeling Global Lightning Distributions in a General Circulation Model
548 *Monthly Weather Review* **122** 1930-9
- 549 Randerson J T, Chen Y, van der Werf G R, Rogers B M and Morton D C 2012 Global burned area and
550 biomass burning emissions from small fires *Journal of Geophysical Research: Biogeosciences*
551 **117**
- 552 Rayner N A, Parker D E, Horton E B, Folland C K, Alexander L V, Rowell D P, Kent E C and Kaplan A
553 2003 Global analyses of sea surface temperature, sea ice, and night marine air temperature since
554 the late nineteenth century **108**
- 555 Schmidt G A, Kelley M, Nazarenko L, Ruedy R, Russell G L, Aleinov I, Bauer M, Bauer S E, Bhat M
556 K, Bleck R, Canuto V, Chen Y-H, Cheng Y, Clune T L, Del Genio A, de Fainchtein R, Faluvegi
557 G, Hansen J E, Healy R J, Kiang N Y, Koch D, Lacis A A, LeGrande A N, Lerner J, Lo K K,
558 Matthews E E, Menon S, Miller R L, Oinas V, Olosa A O, Perlwitz J P, Puma M J, Putman W
559 M, Rind D, Romanou A, Sato M, Shindell D T, Sun S, Syed R A, Tausnev N, Tsigaridis K,
560 Unger N, Voulgarakis A, Yao M-S and Zhang J 2014 Configuration and assessment of the GISS
561 ModelE2 contributions to the CMIP5 archive *Journal of Advances in Modeling Earth Systems*
562 **6** 141-84
- 563 Shindell D T, Faluvegi G, Unger N, Aguilar E, Schmidt G A, Koch D M, Bauer S E and Miller R L 2006
564 Simulations of preindustrial, present-day, and 2100 conditions in the NASA GISS composition
565 and climate model G-PUCCINI *Atmos. Chem. Phys.* **6** 4427-59
- 566 Sofiev M, Ermakova T and Vankevich R 2012 Evaluation of the smoke-injection height from wild-land
567 fires using remote-sensing data *Atmos. Chem. Phys.* **12** 1995-2006

568 Twomey S 1974 Pollution and the planetary albedo *Atmospheric Environment (1967)* **8** 1251-6

569 van der Werf G R, Randerson J T, Giglio L, van Leeuwen T T, Chen Y, Rogers B M, Mu M, van Marle

570 M J E, Morton D C, Collatz G J, Yokelson R J and Kasibhatla P S 2017 Global fire emissions

571 estimates during 1997–2016 *Earth Syst. Sci. Data* **9** 697-720

572 Veira A, Kloster S, Schutgens N A J and Kaiser J W 2015 Fire emission heights in the climate system –

573 Part 2: Impact on transport, black carbon concentrations and radiation *Atmos. Chem. Phys.* **15**

574 7173-93

575 Venevsky S, Thonicke K, Sitch S and Cramer W 2002 Simulating fire regimes in human-dominated

576 ecosystems: Iberian Peninsula case study *Global Change Biology* **8** 984-98

577 Wagner V 1987 *Development and structure of the Canadian Forest Fire Weather Index System, Forestry*

578 *Technical Report: Canadian Forestry Service)*

579 Walter C, Freitas S R, Kottmeier C, Kraut I, Rieger D, Vogel H and Vogel B 2016 The importance of

580 plume rise on the concentrations and atmospheric impacts of biomass burning aerosol *Atmos.*

581 *Chem. Phys.* **16** 9201-19

582 Ward D S, Kloster S, Mahowald N M, Rogers B M, Randerson J T and Hess P G 2012 The changing

583 radiative forcing of fires: global model estimates for past, present and future *Atmos. Chem. Phys.*

584 **12** 10857-86

585 Warren S G and Wiscombe W J 1980 A Model for the Spectral Albedo of Snow. II: Snow Containing

586 Atmospheric Aerosols %J *Journal of Atmospheric Sciences* **37** 2734-45

587 Xu L, Zhu Q, Riley W J, Chen Y, Wang H, Ma P-L and Randerson J T 2021 The Influence of Fire Aerosols

588 on Surface Climate and Gross Primary Production in the Energy Exascale Earth System Model

589 (E3SM) *Journal of Climate* **34** 7219-38

590 Yan H, Zhu Z, Wang B, Zhang K, Luo J, Qian Y and Jiang Y 2021 Tropical African wildfire aerosols

591 trigger teleconnections over mid-to-high latitudes of Northern Hemisphere in January

592 *Environmental Research Letters* **16** 034025

593 Yu P, Toon O B, Bardeen C G, Zhu Y, Rosenlof K H, Portmann R W, Thornberry T D, Gao R-S, Davis S

594 M, Wolf E T, Gouw J d, Peterson D A, Fromm M D and Robock A 2019 Black carbon lofts

595 wildfire smoke high into the stratosphere to form a persistent plume **365** 587-90

596 Yue X, Strada S, Unger N and Wang A 2017 Future inhibition of ecosystem productivity by increasing

597 wildfire pollution over boreal North America *Atmos. Chem. Phys.* **17** 13699-719

598 Yue X and Unger N 2015 The Yale Interactive terrestrial Biosphere model version 1.0: description,

599 evaluation and implementation into NASA GISS ModelE2 *Geosci. Model Dev.* **8** 2399-417

600 Yue X and Unger N 2018 Fire air pollution reduces global terrestrial productivity *Nature*

601 *Communications* **9** 5413

602 Zhuravleva T B, Kabanov D M, Nasrtdinov I M, Russkova T V, Sakerin S M, Smirnov A and Holben B

603 N 2017 Radiative characteristics of aerosol during extreme fire event over Siberia in summer

604 2012 *Atmos. Meas. Tech.* **10** 179-98

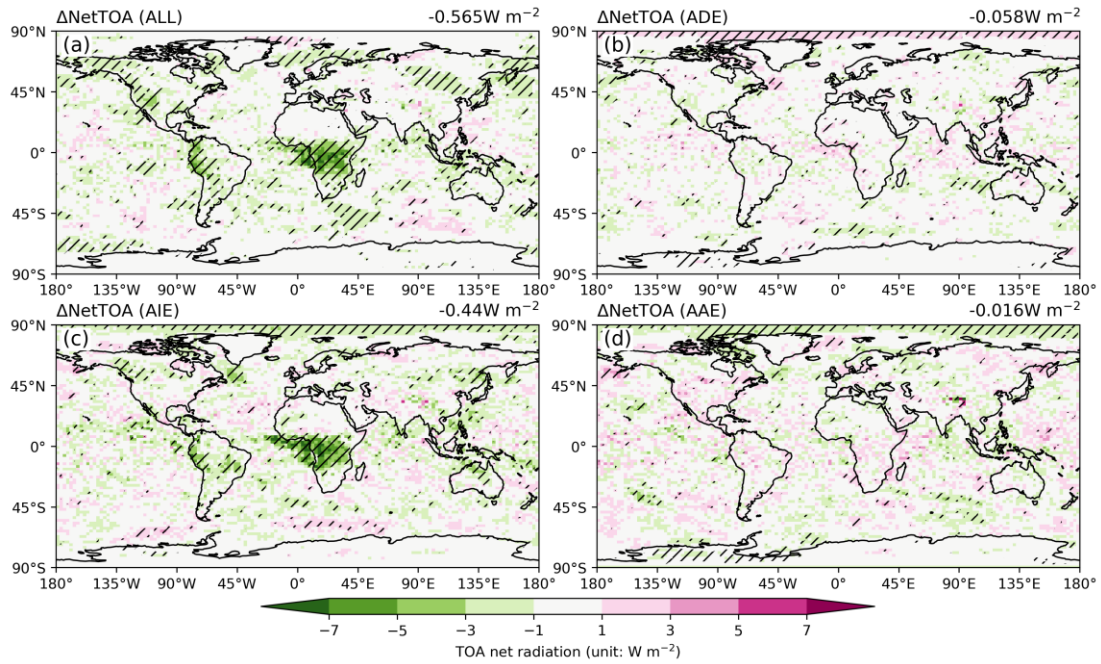
605 Zou Y, Wang Y, Qian Y, Tian H, Yang J and Alvarado E 2020 Using CESM-RESFire to understand

606 climate–fire–ecosystem interactions and the implications for decadal climate variability *Atmos.*

607 *Chem. Phys.* **20** 995-1020

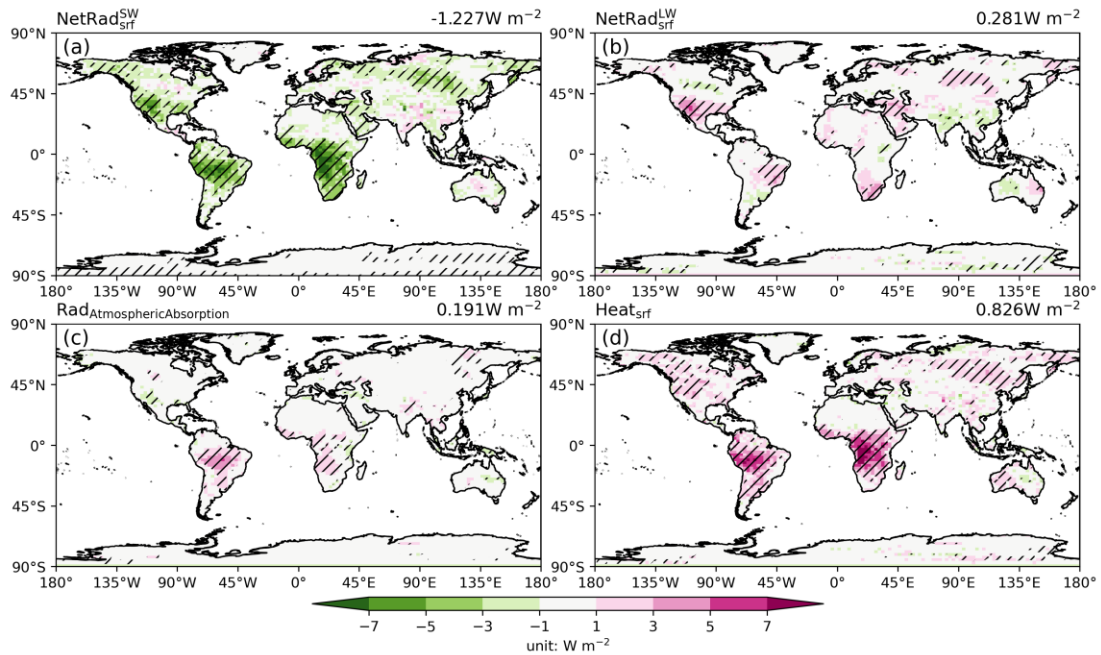
608

609



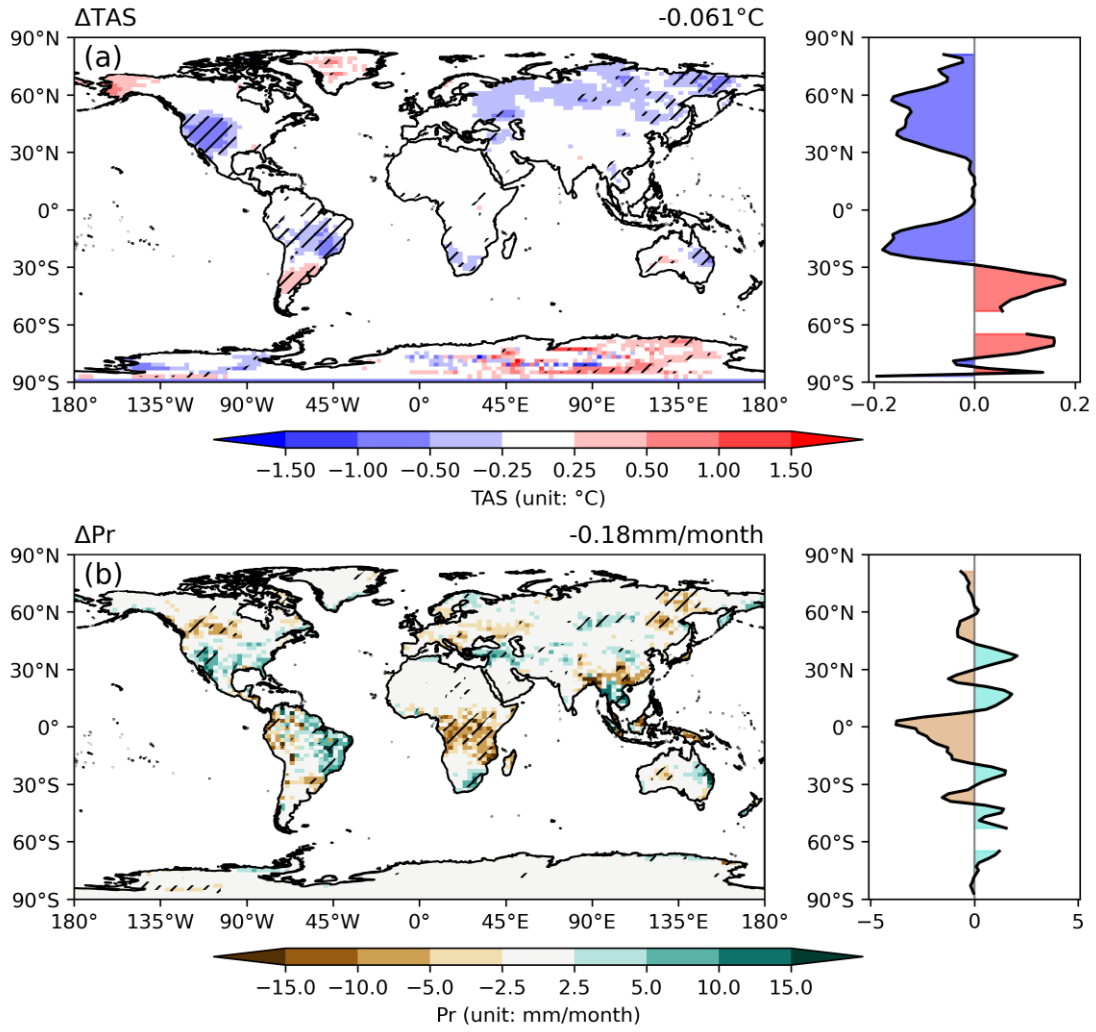
610
 611
 612
 613
 614
 615

Fig. 1 Changes in net radiation flux at top of atmosphere due to (a) total effects, (b) ADE, (c) AIE, and (d) AAE of fire aerosols. Positive values represent the increase of downward radiation. Global average value is shown at the top of each panel. Slashes denote areas with significant ($p < 0.1$) changes.



616
 617
 618
 619
 620
 621
 622

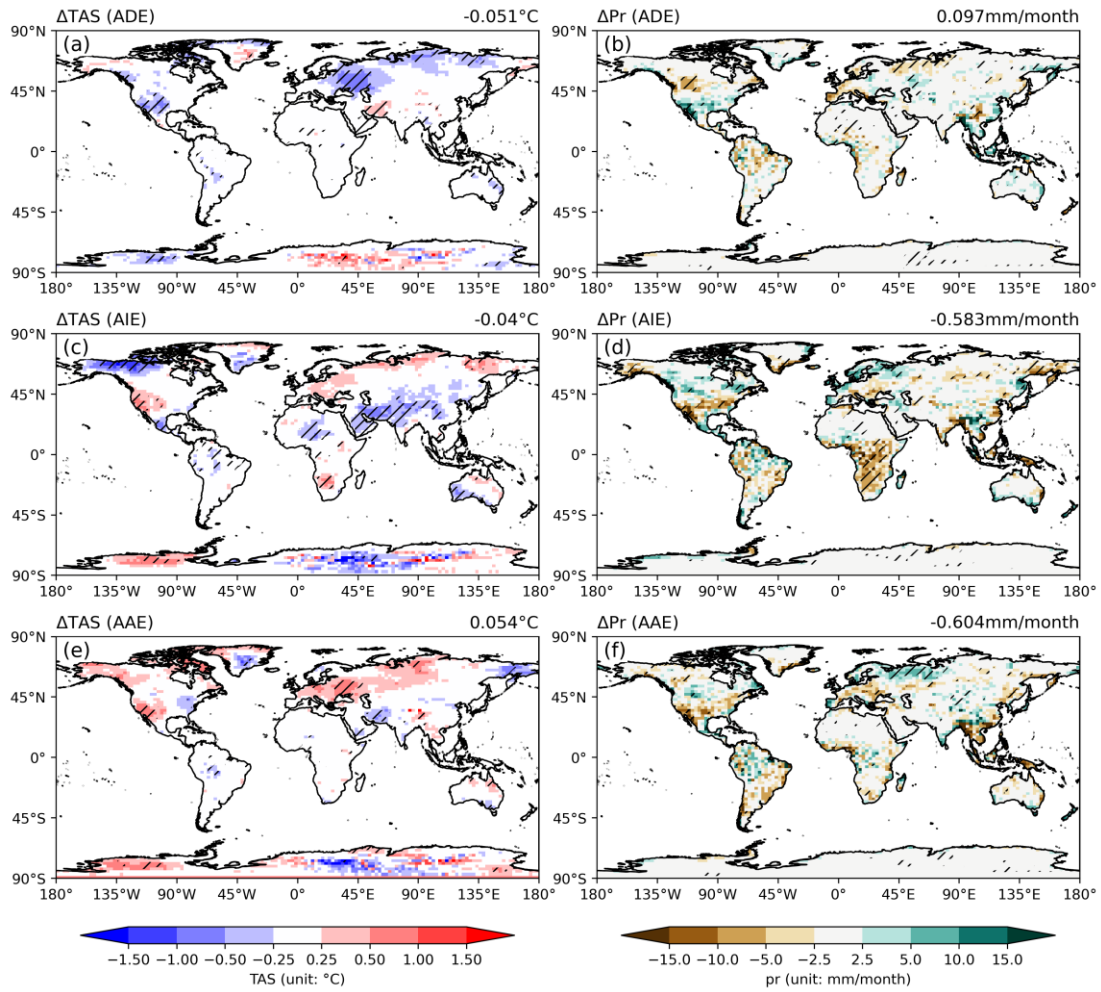
Fig. 2 Changes in (a) surface net shortwave radiation, (b) surface net longwave radiation, (c) atmospheric absorbed radiation, and (d) surface heat flux (sensible + latent) over land grids caused by fire aerosols. Positive values represent the increase of downward radiation/heat for (a, b and d) and absorption for (c). Global land average value is shown at the top of each panel. Slashes denote areas with significant ($p < 0.1$) changes.



623

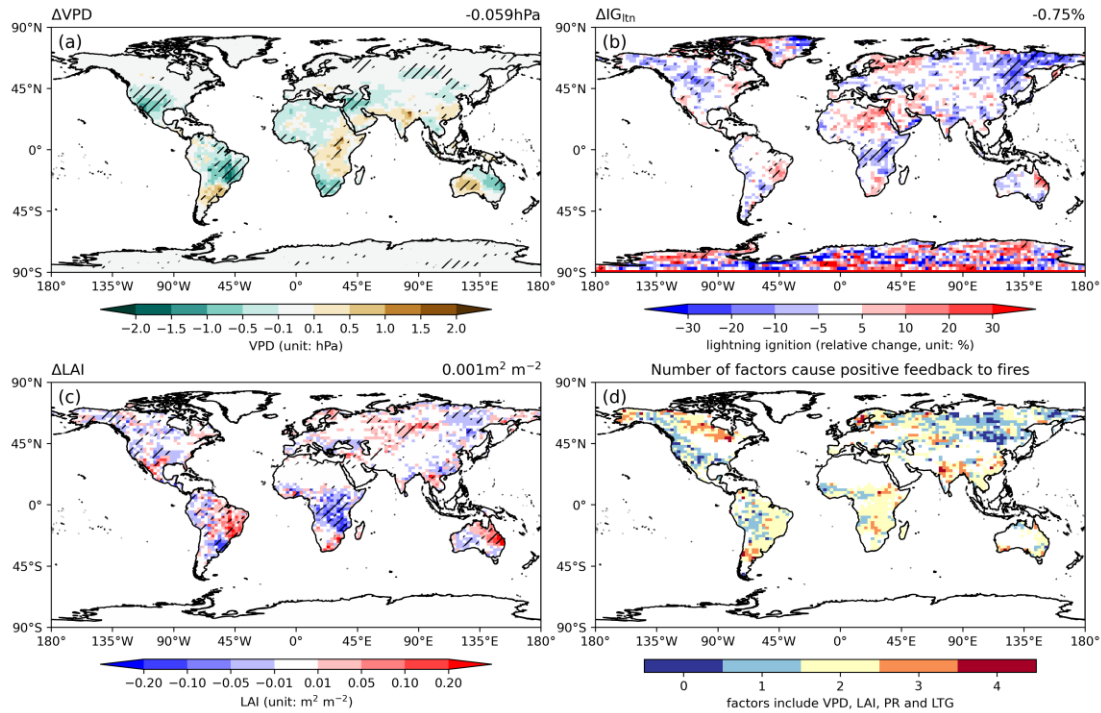
624 **Fig. 3** Changes in (a) surface air temperature and (b) precipitation over land grids caused by fire
 625 aerosols. The zonal averages of these changes are shown by the side of each panel. Global land
 626 average value is shown at the top of each panel. Slashes denote areas with significant ($p < 0.1$)
 627 changes.

628



629
630
631
632
633

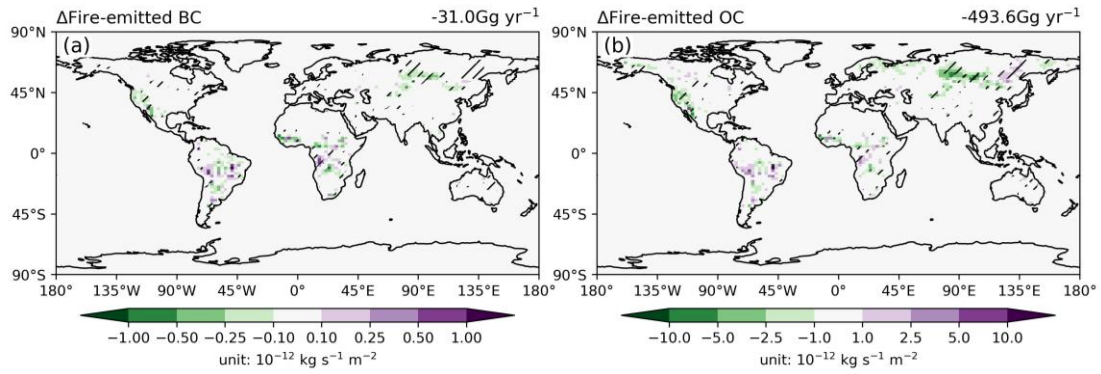
Fig. 4 Changes in (a, c, e) surface air temperature and (b, d, f) precipitation over land grids due to (a, b) ADE, (c, d) AIE, and (e, f) AAE of fire aerosols. Global land average value is shown at the top of each panel. Slashes denote areas with significant ($p < 0.1$) changes.



634

635 **Fig. 5** Changes in (a) vapor pressure deficit (VPD), (b) lightning ignition, and (c) leaf area index
 636 (LAI) over land grids induced by fire aerosols. Global land average value is shown at the top of
 637 each panel. Slashes denote areas with significant ($p < 0.1$) changes. The number of factors whose
 638 changes induced by fire aerosols cause positive feedback to fire emissions is shown in (d). Only
 639 grids with fire-emitted OC larger than $1 \times 10^{-12} \text{ kg s}^{-1} \text{ m}^{-2}$ (colored domain in Fig. S1b) are shown in
 640 (d).

641



642

643 **Fig. 6** Changes in fire emissions of (a) BC and (b) OC through fire-climate interactions. The changes
 644 of fire emissions are calculated as the differences between YF_AD_AI_AA and NF_AD_AI_AA
 645 with slashes indicating significant ($p < 0.1$) changes. The total emission is shown at the top of each
 646 panel.

647

Table 1. Summary of simulations using ModelE2-YIBs

Simulation	Fires ^a	Aerosol direct effect	Aerosol indirect effect	Aerosol albedo effect
NF_AD	No	Yes	No	No
YF_AD	Yes	Yes	No	No
NF_AD_AI	No	Yes	Yes	No
YF_AD_AI	Yes	Yes	Yes	No
NF_AD_AA	No	Yes	No	Yes
YF_AD_AA	Yes	Yes	No	Yes
NF_AD_AI_AA	No	Yes	Yes	Yes
YF_AD_AI_AA	Yes	Yes	Yes	Yes

648

649 ^a All simulations predict fire emissions but the runs with NF do not feed the fire aerosols into the
650 model to perturb radiative fluxes.

651

652 **Table 2.** Comparison of the simulated fire-induced change in radiative forcings at TOA and
 653 surface climate with previous studies

Reference	RF (W m ⁻²)	ADE (W m ⁻²)	AIE (W m ⁻²)	AAE (W m ⁻²)	TAS (°C)	Pr (mm month ⁻¹)
Ward <i>et al.</i> (2012) ^a	-0.55	0.10	-1.00	0.00	—	—
Heald <i>et al.</i> (2014)	—	-0.19	—	—	—	—
Veira <i>et al.</i> (2015)	—	-0.20	—	—	—	—
Grandey <i>et al.</i> (2016)	-1.0	0.04	-1.11	-0.1	—	-0.018
Jiang <i>et al.</i> (2016)	-0.51	0.16	-0.70	0.03	-0.03	-0.3
Zou <i>et al.</i> (2020)	-0.59	-0.003	-0.82	0.19	—	—
Xu <i>et al.</i> (2021)	-0.73	0.25	-0.98	—	-0.17	-1.2
Yan <i>et al.</i> (2021)	-0.62	0.17	-0.74	-0.04	0.03	—
This study	-0.565	-0.058	-0.440	-0.016	-0.061	-0.180

654

655 ^a other effects of fire-induced on radiative turbulances are considered in this paper